Estimating the sea-ice compressive strength from satellite-derived sea-ice drift and NCEP reanalysis data

L.-B. Tremblay
Lamont-Doherty Earth Observatory, Columbia University

M. Hakakian
1 Folie Court, Manhasset, NY 11030, USA.

Submitted to Journal of Physical Oceanography

Corresponding author address:

L.-B. Tremblay, Lamont-Doherty Earth Observatory, Columbia University, 61 Route 9W, Palisades, NY, 10964, USA. (tremblay@ldeo.columbia.edu)

ABSTRACT

Satellite-derived sea-ice drift maps and sea level pressures from reanalysis data are used to infer upper and lower bounds on the large-scale compressive strength of Arctic sea ice. To this end, the two data sets are searched for special situations when the wind forcing and its orientation with respect to the coastline allowed us to deduce a mean sea-ice compressive strength from simple theory. Many estimates of ice compressive strength were possible for the winter of 1992-93 when the Arctic High was confined to the western Arctic and deep penetration of the Icelandic Low produced wind patterns that pushed the ice perpendicular to the coastline in the Beaufort and East Siberian seas. The winter of 1996-97, on the other hand, was characterized by a well established Arctic High, producing wind patterns that generally pushed ice along coastlines rather than against them. Results show lower and upper bounds on the sea-ice compressive strength parameter of 30 and 40 kN m^{-2}, and 35 and 45 kN m^{-2}, for the winters of 1992-93 and 1996-97 respectively (with a potential bias low of about 10 kN m^{-2}). We also found a tensile strength for sea ice of about 25 kN m^{-2} in the East Siberian Sea in the first few hundred km from the land, presumably associated with land fast ice. The proposed mean ice compressive strength estimate is higher than those derived by minimizing the cumulative error between simulated and observed buoy drift trajectories. We note that the uncertainties in the estimates derived from models are large (with an unbiased estimate of standard deviation of 8.75 KN m^{-2}). The estimates of yield strength in isotropic compression presented herin are in good agreement with a previous estimate made during the Arctic Ice Dynamic Joint EXperiment, and with in-situ ice compressive stress measurements made in the Beaufort Sea.

1. Introduction

The advection of sea ice by surface wind and ocean stresses is a fundamental process affecting the concentration and thickness distribution of sea ice at high latitudes. These two factors in turn control the surface albedo, mediate the heat and freshwater fluxes between the atmosphere and ocean (and between different ocean basins), and through multiple feedbacks have a large influence on the high latitude climate. For instance, projections of future climate change have often shown important changes at high latitude (Houghton et al. 2001), in part due to differences in the advection of sea ice. Furthermore anomalies in sea-ice concentrations have been shown to have an effect on the mid-latitude climate variability (Parkinson et al. 2001). Thus, an appropriate treatment of the sea-ice dynamics in regional and global models is crucial in order to properly account for the effects of sea ice on the high latitude climate and its variability.

Important controls on the motion of sea ice include the parameters that govern its strength, and the rheology which specifies the relationship between the internal ice stresses (induced by winds and ocean currents) and the resulting deformation field. In particular, the stiffness of the pack ice is strongly dependent on its compressive and shear strengths, and to a much smaller extent on its tensile strength. These parameters set the shear and compressive loads required for the ice to fail and start to flow. Their relative magnitude will dictate the proportion of axial and shear strain rates present in the sea-ice field (i.e. formation of ridges or flow along slip lines), and also the partition of the energy input from the wind between potential and kinetic energy of the pack, and energy dissipated during such deformations. For these reasons, the specification of the sea-ice compressive and shear strength parameters will have an influence on the simulated thickness distribution, lead fraction, the motion of sea ice, and ultimately on the amount of sea-ice (or fresh water) export out of the Arctic into the northern North Atlantic.

There are two main parameters used to define the compressive strength of sea ice:

the yield strength in isotropic compression (p^*, Coon et al. 1974) and the compressive strength parameter (P^*, Hibler 1979)[1]. A first attempt at independently assessing the yield strength of sea ice in compression was made in the mid-seventies by equating the rate of plastic work done during deformation (i.e. internal stress times strain rate or stretching) to the rate of change of gravitational potential energy and frictional dissipation during the the ridging process (Rothrock 1975). The results suggested a yield strength in isotropic compression p^* appoximately equal to 2 kN m^{-1} for 2 m ice thickness. Shortly after, Pritchard (1976, hereafter referred to as P76) derived a p^* value of about 100 kN m^{-1} for sea ice in the Beaufort Sea using ice drifts and wind measurements from the Arctic Ice Dynamic Joint Experiment (AIDJEX). In this approach, a lower bound on p^* was derived by integrating the surface wind stress over the fetch and using the fact that the ice was not deforming under the applied load. Later Pritchard (1981) added a shearing energy sink to the analysis presented by Rothrock (1975), and the resulting ice strength estimate was now in line with that of P76. Direct sea-ice stress measurements made on ice floes in the Beaufort Sea show peak values in $\sigma_2 - \sigma_1$ (twice the maximum shear stress) ranging between 60 and 100 kN m^{-2} (Richter-Menge et al. 2002a; Richter-Menge and Elder 1998; Richter-Menge et al. 2002b) in general agreement with P76 - assuming that the maximum compressive stress is of the same order of magnitude as the maximum shear stress. More recently, an indirect

---

[1] p^* is one of three parameters defining the shape of a given yield curve - the other two being the stress invariants σ_I and σ_{II}, or the principal stresses σ_1 and σ_2. p^* defines the size of the yield curve but has no effect on its shape. In Hibler (1979), p^* and P^* are referred to as P and P^* respectively. Assuming a linear deformation law, the relationship between the two variables in the standard viscous plastic rheology can be expressed as $p^* = P^* h \exp(-C(1-A))$, or $P = P^* h \exp(-C(1-A))$, where A is the sea-ice concentration.

assessment of the sea-ice compressive strength parameter (P^*) was done by adjusting the value of P^* until the error between the simulated and buoy drift trajectories was a minimum. Using this approach values of 15 kN m^{-2} (Kreyscher et al. 1997) and 27.5 kN m^{-2} (Hibler and Walsh 1982) were obtained for the standard viscous plastic rheology of Hibler (1979). While the range in model-derived P^* is large, depending among other things on the surface wind stresses used to force the models, these estimates are in general agreement with the value derived from the AIDJEX observations (assuming a typical ice thickness of 3 m north-west of Banks Islands in February and a linear deformation law).

Recently, the polar remote sensing group of the Jet Propulsion Laboratory have compiled almost a decade of satellite-derived winter sea-ice drifts for the Arctic, Weddell and Ross seas (using passive microwave imagery SSM/I, Kwok et al. 1998). In the following, satellite-derived sea-ice drift data, and sea level pressures (SLP) from the NCEP reanalysis are used to extend previous estimates of sea-ice strength made during AIDJEX. Using this approach, we make a large number of ice strength estimates from which a range of possible value for both p^* and P^* can be made. The outline of the manuscript is as follows. Section 2 presents the rationale and method used to derive the sea-ice strength estimates. In section 3 we presents results for the winters of 1992-93 and 1996-97 for the Arctic Ocean. The main conclusions drawn from this study are summarized in section 4.

2. Method

The methodology used to derive sea-ice strength estimates follows that presented in P76. In order to provide an independent measure of p^* and P^*, as well as additional constraints on the selection of this parameter (i.e. upper and lower bounds), 3-day average sea-ice drift velocities from passive microwave satellite imagery and sea level pressure maps (2.5 x 2.5 degree spatial resolution and one day temporal resolution) from

the NCEP reanalysis are analyzed.

a. Upper and Lower bounds estimates

In the Arctic, sea ice drifts on average approximately 5 degrees to the right of the geostrophic winds in winter (Thorndike and Colony 1982). In the atmospheric boundary layer, the winds turn to the left (due to surface friction). However, the sea-ice drift is to the right of the surface wind due to the Coriolis effect. For typical ice thickness, drift speed, and internal ice stresses, these two effects almost compensate one another and the ice flow nearly follows the geostrophic winds and therefore lines of constant sea level pressure (see Fig. 1, or Kwok et al. 1998, their Fig. 2). Of course, large cross isobar sea-ice flow (to the left or the right) also occurs depending on the relative importances of wind stress, water drag (including wind and water turning angles), the Coriolis effect and the sea-ice interaction term (Steele et al. 1997). An example of this is seen in the Laptev Sea, where the sea-ice drift is to the right of the isobars (see Fig.1). In the following, we consider large scale sea-ice motion for which the geostrophic approximation is a good first approximation. FIG. 1.

In a first step, instances when the wind blew perpendicular to a coastline for a few consecutive days were identified and recorded. If the ice does not deform under such a condition, the surface wind stress must be balanced by the divergence of the internal ice stress, the water drag and the sea surface tilt term. Assuming that (1) the geostrophic ocean current is negligible (i.e. ocean stress and sea surface tilt terms are ignored – errors associated with this assumption are discussed at the end of this section), and that (2) the forcing is uniform in space ($\partial/\partial y = 0$), the momentum balance in the direction of the flow (x) can be written as (P76):

$$\tau_x = -\frac{\partial \sigma_{xx}}{\partial x}, \tag{1}$$

where τ_x is the wind stress and σ_{xx} is the axial component of the sea-ice stress tensor

acting in the x-direction. Integrating over the fetch of the wind L, and considering the fact that σ_{xx} is always negative, we obtain:

$$-\sigma_{xx}(L) \;=\; -\sigma_{xx}(0) + \tau_x L \;>\; \tau_x L. \tag{2}$$

Since the axial stress is by definition smaller (in magnitude) than the maximum normal stress (expressed in terms of the stress invariant components as $-\sigma_I + \sigma_{II}$), then

$$-\sigma_I + \sigma_{II} \;>\; \tau_x L\,. \tag{3}$$

In this equation, σ_I and σ_{II} represent the average normal stress and maximum shear stress at a point, and can be related to one another for a given choice of yield curve.

For an elliptical and a Mohr Coulomb yield curve, the relationship between the two stress invariants can be written in normalized coordinates as:

$$(\sigma_I^* + 1)^2 + \sigma_{II}^{*2} e^2 \;=\; 1, \qquad \sigma^* = \sigma/(p^*/2) \qquad \text{Ellipse (Ell)}, \tag{4}$$

$$\sigma_{II}^* + \sigma_I^* \sin\phi \;=\; 0, \qquad \sigma^* = \sigma/(p^*) \qquad \text{Mohr Coulomb (MC)}, \tag{5}$$

where e (the ellipse aspect ratio, Hibler 1979) and ϕ (the internal angle of friction, Flato and Hibler 1992; Tremblay and Mysak 1997) give a measure of the sea-ice resistance to shear deformation. Using Eq. 4 and 5, the maximum compressive strength ($-\sigma_I + \sigma_{II}$) can be written as:

$$\max|-\sigma_I^* + \sigma_{II}^*| \;=\; 1 + \sqrt{1 + 1/e^2}, \;\; \max|-\sigma_I + \sigma_{II}| = \frac{1 + \sqrt{1 + 1/e^2}}{2} p^*, \;\text{Ell}, \tag{6}$$

$$\max|-\sigma_I^* + \sigma_{II}^*| \;=\; 1 + \sin\phi, \qquad \max|-\sigma_I + \sigma_{II}| = (1 + \sin\phi) p^*, \qquad \text{MC}. \tag{7}$$

Note that the maximum compressive strength for the elliptical yield curve is relatively insensitive to the ellipse aspect ratio, ranging from a value of 2.414 for a circular yield curve ($e = 1$) to 2 for the cavitating fluid rheology ($e \to \infty$) - values quoted are in non-dimensional form. For a typical e value of 2, the maximum compressive strength is equal to 2.118. In Eq. 6, the maximum (in magnitude) normal stress occurs at

$\sigma_I^* = \sigma_I/(p^*/2) = -1 - e/\sqrt{1+e^2}$. For the Mohr Coulomb yield curve (Eq. 7), the maximum normal stress occurs at $\sigma_I^* = \sigma_I/p^* = -1$.

Combining Eqs. 3, 6 and 7, a lower bound on the compressive strength of sea ice can expressed as:

$$p^* > \frac{1}{\alpha}\tau_x L, \qquad \text{where} \quad \alpha = \begin{cases} (\,1+\sqrt{1+1/e^2}\,)/2 & \text{Ell,} \\ 1+\sin\phi & \text{MC,} \end{cases} \tag{8}$$

In the above equation, $\tau_x L$ represents the total force exerted by the wind over the fetch, and α is a rheology dependent parameter relating the maximum normal stress at a point and the isotropic yield strength of the material in compression. This parameter is expressed as a function of the internal angle of friction ϕ, for the Mohr-Coulomb yield curve (typically equal to 30°), and the ellipse aspect ratio e for the elliptical yield curve (typically equal to 2). In the following, results will be presented for a value of $\alpha = 1.0$, representative of the elliptical yield curve ($\alpha \approx 1.1$ for $e = 2$), and cavitating fluid rheology ($\alpha = 1$ for $e \to \infty$). For the Mohr-Coulomb yield curve, $\alpha = 1.5$ and the estimates of p^* and P^* presented later can simply be scaled down by this factor.

In a similar manner, an upper bound on the compressive strength of sea ice is derived for cases when the ice deforms under the applied load. In this case, neglecting the ocean stress (a force retarding the motion of the ice) reverses the sign of the inequality in equation 2, so long as the axial stress at the beginning of the fetch $\sigma_{xx}(0)$ is small compared to $\tau_x L$. Considering only cases when the shear stress (σ_{xy}) in the region of interest is small (i.e. $-\sigma_{xx} \approx -\sigma_{yy} \approx -\sigma_I >> \sigma_{II}$), equation 3 provides us with an upper bound on the sea-ice compressive strength equal to:

$$-\sigma_I + \sigma_{II} \;\; \approx -\sigma_I \;\; < \;\; \tau_x L\,, \tag{9}$$

and equation 8 still holds with the sign of the inequality reversed. Note that the assumption of small $\sigma_{xx}(0)$ and σ_{xy} leads to an error of the same sign on the left and right hand sides of equation 2, and will tend to cancel one another out. Using a standard

bulk formula (e.g., McPhee 1975), the surface wind stress acting on the ice $\boldsymbol{\tau_a}$ can be written as:

$$\tau_a \;\; = \;\; \tau_x \boldsymbol{i} + \tau_y \boldsymbol{j} = \rho_a C_{da} \, |U_a|^2 (\cos\theta \;\; \boldsymbol{i} + \sin\theta \;\; \boldsymbol{j}),$$

where ρ_a (= 1.3 kg m^{-3}) is the air density, C_{da} (= 0.0012, Hibler 1979) is the air-ice drag coefficient, U_a is the mean geostrophic wind over the fetch L (estimated from the SLP gradient), and θ (= 25°) is the wind turning angle.

Assuming a deformation law of the form (Hibler 1979):

$$p^* = P^* h, \tag{10}$$

where h is the thickness of the weakest ice over the fetch L, an estimate of the sea-ice strength parameter P^* can be deduced from the yield strength in isotropic compression p^*. In the following, we specify h from the seasonal ice thickness climatology of Bourke and Garrett (1987). Sea-ice thickness from a high resolution simulation of the Arctic Ocean forced with contemporaneous atmospheric data (Armstrong et al. 2003) did not lead to any significant differences in the results (not presented here). Ice thickness estimates derived from altimeter measurements in the peripheral seas of the Arctic are starting to emerge (Laxon et al. 2003). When they become available, observed ice thickness can be used to further test this method.

There are several sources of uncertainties associated with this approach. Neglecting the geostrophic ocean current decreases the ice strength estimates by about 15% (assuming typical values of ocean currents are less than 5 cm s^{-1}, P76). Large uncertainties can be associated with the choice of air-ice drag coefficient. Prinsenberg and Peterson (2002) and Smith (1990) report values of C_{da} over ice surfaces ranging from 0.5 to 5×10^{-3} depending on the atmospheric boundary layer stability and surface roughness. The uncertainty on the mean drag coefficient over large fetches is likely to be much smaller, but results from modeling studies suggest that it may still be large -

see discussion in section 3. The geostrophic wind speed derived from NCEP reanalysis SLP at high latitude is usually underestimated by about 8% (This bias however is not significant, Cullather and Lynch 2003; Smith et al. 2001; Wylie 2001). This may translate into an underestimation of the wind stress by about 15%. Errors in wind direction are also present. Francis and Hunter (2005) report 0.5 and 0 m s^{-1} errors in the zonal and meridional components of the surface winds. Given that all events analyzed in this study have a dominant meridional component (perpendicular to a coastline) and assuming a mean wind speed of 5 m s^{-1} in the Beaufort (estimated using data from the Surface HEat Budget of the Arctic - SHEBA - experiment), this gives an error of about 5 degrees in the wind direction which amounts to an error of less than 1 % in surface stresses. The measurement of the fetch is relatively precise when compared to other fields. Finally, errors of plus or minus 50 cm in sea-ice thickness estimates of level ice in the peripheral seas of the Artic was assessed based on the output of a 50-year sea-ice model run by Armstrong et al. (2003). This amounts to approximately 25 to 40 % of the mean ice thickness for the Beaufort and East Siberian-Laptev seas respectively. In October 1997, when the camp for the SHEBA experiment was set up in early winter, sea-ice thickness in the Beaufort Sea was approximately 1 meter thinner than expected based on thickness measurements made during the AIDJEX field campaign in the same region in the mid seventies (McPhee et al. 1998), in general agreement with the model estimates.

In P76, one estimate of sea-ice yield strength in isotropic compression was derived from four events that occurred in February 1976 during AIDJEX. In the present study, a large number of estimates of sea-ice strength is used to derive ranges of possible values for p^* and P^*. Our large sampling technique minimizes the sensitivity of the results to random errors in wind stress and sea-ice thickness. The uncertainty in the final numbers quoted in the next section therefore depends mainly on correlated errors and biases present in those two input fields.

b. Scene identification

Criteria for selecting sea-ice drift events are summarized as follows:

- The wind should be blowing consistently in the same direction and perpendicular to a coastline. The word "consistently" in this context depends on the wind history prior to the events. If the wind was recently blowing sea ice away from the coast, thin ice will be present in the pack, and the first several hours will be used to ridge the newly formed ice in the leads. In this case we require that the wind be blowing consistently for a couple of days before sea-ice strength estimates are performed. Again the spatial and temporal scales associated with the geostrophic winds used in this study are 1 days and of the order of 100km, respectively.
- The wind should be blowing in the same direction over the entire fetch. Large changes in the direction of the winds will induce shear deformation and the normal load may not be transmitted all the way to the coastline. Such a case would lead to very low ice strength lower bound estimates that are not applicable.

The selected events are used to derive strength estimates using sea-ice drift data (to determine whether deformation is present or not) and sea level pressure from NCEP reanalysis (to determine the forcing on the ice).

3. Results

Most events used in this study are from the Beaufort, East Siberian, and Laptev seas. The number of events for the winter of 1992-93 is much larger than for the winter of 1996-97. In 1992-93, the winter was characterized by a deep penetration of low pressure systems into the eastern and central Arctic with a small Arctic High confined to the Beaufort Sea (typical of positive NAO years in recent decades). This was generally true except sometimes in April and May when the Arctic high occupied the whole Arctic, and in late February when low pressure systems entering from the northern

North Pacific occupied a large fraction of the Beaufort and Chukchi seas. During that year the dominant atmospheric circulation pattern was such that ice was often blown perpendicular to the coastline in the Beaufort and East Siberian seas, providing good conditions for ice strength estimates. In 1996-97, on the other hand, the Arctic High often had a col pattern (saddle point) with one lobe over Siberia and another over the Canadian Arctic Archipelago (CAA), or a High occupying the entire central Arctic, as in December and February. These wind patterns often produced very low winds along coastlines or high winds that were more or less parallel to coastlines and thus were less conducive to sea-ice strength estimates.

Figs. 2, 3 and 4 show the results from the analysis of the daily maps for the winters of 1992-93 and 1996-97. This analysis has provided more than 100 lower and upper bound estimates of the sea-ice compressive and tensile strength parameters (for a value of $\alpha = 1.0$). The estimates are lumped in bins of 5 kN m^{-2} (or 10 kN m^{-1} for p^*) ranging from -30 kN m^{-2} (tensile) to more than 100 kN m^{-2} (compressive), and the total number of estimates in each bin was recorded. In this analysis, upper bound estimates were also included. These were possible because in most cases considered, the ice was pushed against two perpendicular coastlines (e.g. those of Banks Island, and the Yukon and Alaskan coastlines) and consequently the shear stress within the ice is believed to be relatively small.

FIG. 2.

FIG. 3.

FIG. 4.

The estimates of yield strength in isotropic compression (p^*) for all cases recorded in the Beaufort Sea (when ice was pushed against the Alaskan coast or Banks Island) for peak winter are shown in Fig. 2. The results show a range of possible p^* between 90 and 130 kN m^{-1}, in general agreement with a previous peak winter estimate in the same region made by P76 (100 kN m^{-1}). The estimates of yield strength in isotropic compression are also in general agreement with in-situ ice compressive stress measurements made in the Beaufort Sea by Richter-Menge et al. (2002a, b) and Richter-Menge and Elder (1998). The range in p^* is somewhat large as sea ice of varying

thickness is present north of the Alaskan coast and Banks Island. Thicker ice will support larger loads before deformation occurs and will provide larger p^* estimates (and vice versa).

Figs. 3 and 4 show lower and upper bound estimates of the compressive strength parameter (P^*). The results for both years are consistent, showing ranges of possible P^* values between 30 and 40 kN m^{-2} for the winter of 1992-93, and 35 and 45 kN m^{-2} for the winter of 1996-97. Cases where off-shore winds did not cause sea-ice deformation were also recorded. These cases were observed mainly in the East Siberian Sea. The results show ice tensile strengths over a couple of hundred km of presumably land fast ice of about 25-30 kN m^{-2} (Fig. 3a).

The sensitivity of the sea-ice strength estimates to random errors in sea-ice thickness (Eq. 10) is small. To quantify this, the same analysis was repeated using the seasonal ice thickness climatology of Bourke and Garrett ± a random error of 50 cm (see end of section 2.1). This affected the shape of the distributions, but had no noticeable effect on the range of allowable P^* presented in Figs. 3 and 4 - due to the large number of events analyzed. Of course, the error may not be random: i.e. there could be biases present in one given year. The fact that the analysis of two separate years (1992-93 and 1996-97) with two very different wind patterns in the Arctic give very similar ranges of P^* suggests that the uncertainties associated with the choice of ice thickness are comparable to the range quoted for the P^* estimates (15 kN m^{-2}). The neglect of ocean currents however, is believed to lead to a 15 % underestimate of the sea-ice strength. The bias low in the NCEP SLP is not significant and therefore is not believed to lead to any significant uncertainty in the range of possible ice strength esimates.

The range of possible P^* shown in Figs. 3 and 4 are of the same order of magnitude as previous estimates of 15 kN m^{-2} by Kreyscher et al. (1997, 2000) and 27.5 kN m^{-2} by Hibler and Walsh (1982). Note, however, the large difference in P^* values between the two studies. In both papers, the optimal P^* is found by minimizing the error between

buoy trajectories and the simulated sea-ice drift from the same locations. Kreyscher et al. (2000) use a value of C_{da} of 2.75×10^{-3} and surface winds from the NCEP/NCAR reanalysis, while Hibler and Walsh (1982) uses a C_{da} of 1.2×10^{-3}, together with geostrophic wind derived from the NCAR SLP. On average, the NCEP reanalysis surface winds in winter in the Arctic are 10% smaller than the geostrophic winds in the free troposphere. This leads to 20 % smaller wind stresses, and is not enough to compensate for the large difference in the air-ice drag coefficients used between the two studies (2.75 versus 1.2 $\times 10^{-3}$). The disparity is also compounded by the fact that the P^* of Kreyscher et al. (2000) is also smaller, despite the larger C_{da}.

Other factors could explain the difference between the two studies, namely: the grid resolution, the buoy data used to minimize the error [the buoy statistics used by Hibler and Walsh are based on 2 years of data, while those of Kreyscher et al. are based on 16 years of data], and the simulated ice thickness (the ice thickness in Hibler and Walsh (1982) is slightly thinner in the central Arctic than that of (Kreyscher et al. 2000)). These differences however are not expected to have a large impact on the evaluation of P^*. Finally both models may not have been iterated until convergence is achieved - for instance running a model with a smaller pseudo time step will have an impact on the stress state produced by the model (Zhang and Rothrock 2000) and the mean kinetic energy of the pack ice (results not shown).

At this point, one thing stands out. The optimal value of P^* that should be used in model simulations is intimately linked with the choice of air-ice drag coefficient (i.e. higher energy input from winds, higher energy dissipation is required). Uncertainties in the air-ice drag coefficient are therefore a major source of error in trying to evaluate the appropriate P^* to be used in a model study. In our study we calculate the wind stress following Hibler (1979) or Hibler and Walsh (1982), and accordingly our estimates should be compared with the value of 27.5 kN m^{-2}. Taking into account the errors associated with both method of arriving at P^* estimates, we consider the estimate

shown in Fig. 3 and 4 to be generally higher than values quoted in the literature. This is reasonable, in part since prior studies use models forced with daily-averaged winds (where wind gusts are filtered). In order to mimic the behavior of real ice, a smaller ice strength in models would be required to compensate for this.

4. Concluding remarks and future work

Sea-ice drift maps and sea level pressure data from passive microwave imagery and the NCEP reanalysis were used to infer the large-scale compressive strength of sea ice. To this end, we identified instances when the wind was blowing over sea ice for a few consecutive days perpendicular to a coastline, during the winters of 1992-93 and 1996-97. Using standard bulk formula, the total force acting on the ice was calculated from the fetch and the mean wind speed acting over that fetch. Results show a possible range of sea-ice compressive strengths between 30 and 45 kN m^{-2}, an estimate valid for both elliptical and the cavitating fluid rheologies. For the Mohr Coulomb yield curve these values are smaller by a factor of 1.5. The P^* estimates are in general agreement but are somewhat larger in magnitude than values derived from the calibration of sea-ice models against sea-ice drift from buoy data (forced with daily averaged wind). Note however that the uncertainty in model derived P^* using method is large. The range of values for the yield strength in isotropic compression is also in close agreement with a previous estimate made by Pritchard (1976) during AIDJEX in the Beaufort Sea, and with in-situ stress measurements made in the Beaufort Sea. Future work will include similar estimates for the Southern Ocean, where passive microwave imagery and reanalysis data are also available. Furthermore, as sea-ice thicknesses derived from altimater data are starting to become available, these observations will be used in conjunction with the method presented here to provide P^* estimates.

Acknowledgment.

We thank Robert Pritchard for numerous useful discussions and comments during the course of this work, the Jet Propulsion Laboratory for the satellite-derived sea-ice drift data (Ron Kwok), the National Centers for Environmental Prediction (NCEP) for the sea level pressure reanalysis data, and Jean-Francois Lemieux for carefully reading the final manuscript and suggestions for changes. We are also grateful to Felix Tubiana for his help with the data manipulation and Omar Qureshi for organizing some of the data for the year 1992-93. We would also like to thank one anonymous reviewer and Cathleen Geiger for their careful reviews of the manuscript. Their comments helped clarified a number of important issues and led to an overall much clearer paper. Finally we thank Katherine Leonard for proofreading the final manuscript. B. Tremblay was supported by National Science Foundation grant OPP98-18711. This work is Lamont-Doherty Earth Observatory contribution # 0000.

REFERENCES

Armstrong, A. E., L.-B. Tremblay, and L. A. Mysak, 2003: A data-model intercomparison study of Arctic sea-ice variability. *Climate Dynamics*, **20**, 465–476.

Bourke, R. H. and R. P. Garrett, 1987: Sea ice thickness distribution in the Arctic Ocean. *Cold Regions Science and Technology*, **13**, 259–280.

Coon, M. D., S. A. Maykut, R. S. Pritchard, D. A. Rothrock, and A. S. Thorndike, 1974: Modelling the pack ice as an elastic plastic material. *AIDJEX Bulletin*, **24**, 1–105.

Cullather, R. I. and A. H. Lynch, 2003: The annular cycle and interannual variability of atmospheric pressure in the vicinity of the North Pole. *International Journal of Climatology*, **23**, 1161–1183.

Flato, G. M. and W. D. Hibler, III, 1992: Modeling pack ice as a cavitating fluid. *Journal of Physical Oceanography*, **22**, 626–651.

Francis, J. A. and E. Hunter, 2005: Arctic tropospheric winds derived from TOVS satellite retrievals. *Journal of Climate, in press*.

Hibler, W. D., III, 1979: A dynamic thermodynamic sea ice model. *Journal of Physical Oceanography*, **9**, 815–846.

Hibler, W. D., III and J. E. Walsh, 1982: On modeling seasonal and interannual fluctuations of Arctic sea ice. *Journal of Physical Oceanography*, **12**, 1514–1523.

Houghton, J. T., Y. Ding, D. J. Griggs, M. Nouger, P. J. van der Linden, X. Dai, K. Maskell, and C. A. Johnson, 2001: *Climate Change 2001: The scientific basis*. Cambridge Univ. Press, New York, 881pp pp.

Kreyscher, M., M. Harder, and P. Lemke, 1997: First results of the Sea-Ice Model Intercomparison Project (SIMIP). *Annals of Glaciology*, **25**, 8–11.

Kreyscher, M., M. Harder, P. Lemke, and G. M. Flato, 2000: Results of the Sea-Ice Model Intercomparison Project: evaluation of sea ice rheology schemes for use in climate simulations. *Journal of Geophysical Research*, **105**, 11299–11320.

Kwok, R., D. A. Schweiger, D. A. Rothrock, S. Pang, and C. Kottmeier, 1998: Assessment of sea ice motion from sequential passive microwave observations with ERS and buoy ice motion. *Journal of Geophysical Research*, **103**, 8191–8214.

Laxon, S., N. Peacock, and D. Smith, 2003: High interannual variability of sea ice thickness in the Arctic region. *Nature*, **425**, 947–950, doi:10.1038/nature02050.

McPhee, M. G., 1975: Ice-ocean momentum transfer for the AIDJEX ice model. *AIDJEX Bulletin*, **29**, 93–111.

McPhee, M. G., T. P. Stanton, J. H. Morison, and D. G. Martinson, 1998: Freshening of the upper ocean in the Arctic: Is perennial sea ice disappearing? *Geophysical Research Letters*, **25**, 1729–1732.

Parkinson, C. L., D. Rind, R. J. Healy, and D. J. Martinson, 2001: The impact of sea ice concentration accuracies on climate model simulations with the GISS GCM. *Journal of Climate*, **14**, 2606–2623.

Prinsenberg, S. and I. K. Peterson, 2002: Variations in air-ice drag coefficient due to ice surface roughness. *International Journal of Offshore and Polar Engineering*, **12**, 121–125.

Pritchard, R., 1981: Mechanical behaviour of pack ice. *Mechanics of Structured Media*, E. Selvadurai, ed., Elsevier, 371–405.

Pritchard, R. S., 1976: An estimate of the strength of Arctic pack ice. *AIDJEX Bulletin*, **34**, 94–113.

Richter-Menge, B. Elder, K. Claffey, J. E. Overland, and S. Salo, 2002a: In-situ sea-ice

stresses in the Western Arctic during the winter of 2001-2002. *Proceeding of the 16th IAHR International Symposium on Ice*, Dunedin, New Zealand, 131–138.

Richter-Menge, J. A. and B. Elder, 1998: Characteristics of pack ice stress in the Alaskan Beaufort Sea. *Journal of Geophysical Research*, **103**, 21817–21829.

Richter-Menge, J. A., S. L. McNutt, J. E. Overland, and R. Kwok, 2002b: Relating arctic pack ice stress and deformation under winter conditions. *Journal of Geophysical Research*, **107**, 8040, doi:10.1029/2000JC000477.

Rothrock, D. A., 1975: Energetics of plastic-deformation of pack ice by ridging. *Journal of Geophysical Research*, **80**, 4514–4519.

Smith, S. R., D. M. Legler, and K. V. Verzone, 2001: Quantifying undertainties in NCEP reanalysis using high-quality research vessel observations. *Journal of Climate*, **14**, 4062–4070.

Smith, W. O., 1990: *Polar Oceanography. Part A: Physical Science*. Academic Press.

Steele, M., J. L. Zhang, D. Rothrock, and H. Stern, 1997: The force balance of sea ice in a numerical model of the Arctic ocean. *Journal Geophysical Research*, **102**, 21061–21072.

Thorndike, A. S. and R. Colony, 1982: Sea ice motion in response to geostrophic winds. *Journal of Geophysical Research*, **87**, 5845–5852.

Tremblay, L.-B. and L. A. Mysak, 1997: Modelling sea ice as a granular material, including the dilatancy effect. *Journal of Physical Oceanography*, **27**, 2342–2360.

Wylie, D. P., 2001: Arctic weather during the FIRE/ACE flights in 1998. *Journal of Geophysical Research*, **106**, 15363–15375.

Zhang, J. and D. Rothrock, 2000: Modeling Arctic sea ice with an efficient plastic solution. *J. Geophys. Res.*, **105**, 3325–3338.

Printed January 19, 2006.

Figure Captions

FIG. 1. Example of sea-ice drift (arrows) derived from passive microwave imagery from the Polar Remote Sensing Group (JPL), and NCEP reanalysis sea level pressures (SLP - 1000mb) for March 16, 1993. The fetch L and the geostrophic wind U_a are also indicated.

FIG. 2. Histogram of lower (a) and upper (b) bound estimates of the sea-ice yield strength in isotropic compression (p^*) for the Beaufort Sea for JFMA of 1992-93, and 1996-97. The thick vertical solid and dashed lines indicate the mean and plus or minus one standard deviation for the p^* distributions. The grey shaded area indicates the range of possible yield strength in isotropic compression derived from the upper and lower bound estimates.

FIG. 3. Histogram of lower (a) and upper (b) bound estimates of sea-ice compressive strength parameter (P^*). These estimates were obtained using satellite-derived sea-ice drift data from the winter (Oct-May) of 1992-93. In the top panel, tensile strength estimates are shown as negative P^*. In this case, lower bound refers to the absolute value of P^*. The thick vertical solid and dashed lines indicate the mean and plus or minus one standard deviation for the P^* distributions. The grey shaded area indicates the range of possible sea-ice compressive strength parameter derived from the upper and lower bound estimates.

FIG. 4. Histogram of lower bound (a) and upper bound (b) estimates of sea-ice compressive strength parameter (P^*). These estimates were obtained using satellite derived sea-ice drift data from the winter (Oct-May) of 1996-97. In the top panel, tensile strength estimates are shown as negative P^*. In this case, lower bound refers to the absolute value of P^*. The thick vertical solid and dashed lines indicate the mean and, plus or minus one standard deviation for the P^* distributions. The grey shaded area indicates the range of possible sea-ice compressive strength parameters derived from the upper and lower bound estimates.

Figures

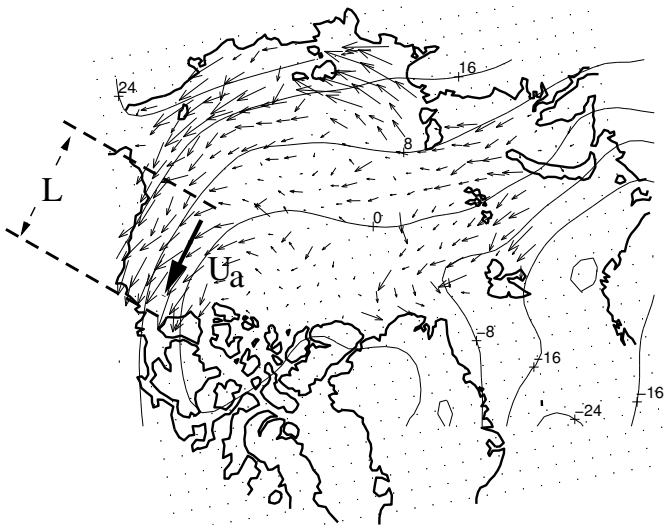

FIG. 1. Example of sea-ice drift (arrows) derived from passive microwave imagery from the Polar Remote Sensing Group (JPL), and NCEP reanalysis sea level pressures (SLP - 1000mb) for March 16, 1993. The fetch L and the geostrophic wind U_a are also indicated.

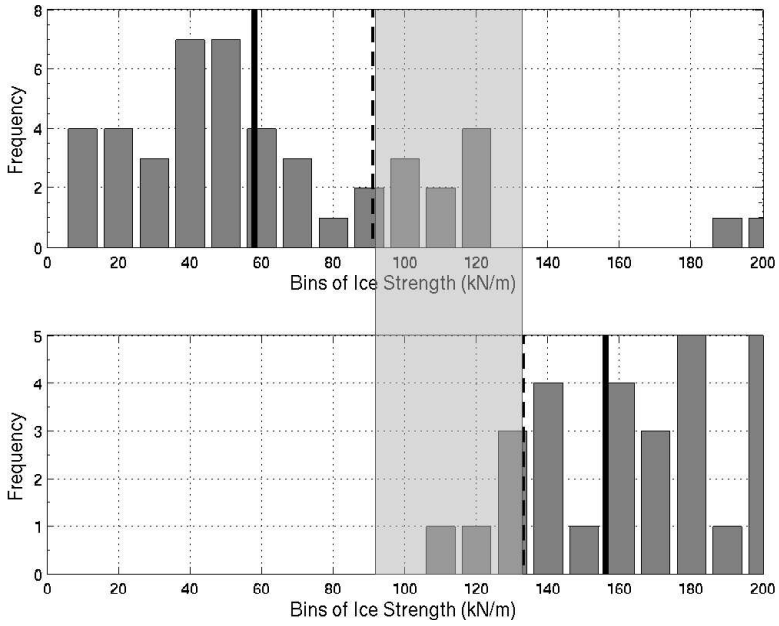

FIG. 2. Histogram of lower (a) and upper (b) bound estimates of the sea-ice yield strength in isotropic compression (p^*) for the Beaufort Sea for JFMA of 1992-93, and 1996-97. The thick vertical solid and dashed lines indicate the mean and plus or minus one standard deviation for the p^* distributions. The grey shaded area indicates the range of possible yield strength in isotropic compression derived from the upper and lower bound estimates.

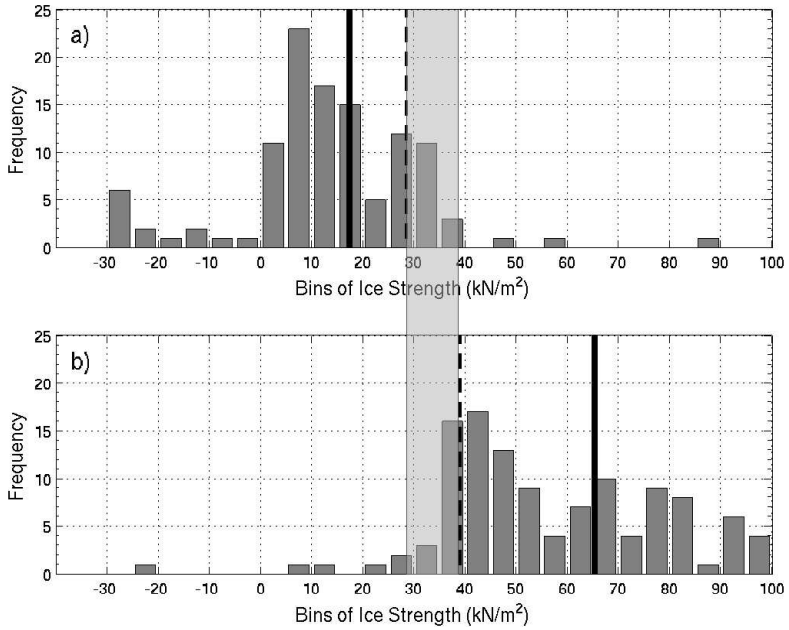

FIG. 3. Histogram of lower (a) and upper (b) bound estimates of sea-ice compressive strength parameter (P^*). These estimates were obtained using satellite-derived sea-ice drift data from the winter (Oct-May) of 1992-93. In the top panel, tensile strength estimates are shown as negative P^*. In this case, lower bound refers to the absolute value of P^*. The thick vertical solid and dashed lines indicate the mean and plus or minus one standard deviation for the P^* distributions. The grey shaded area indicates the range of possible sea-ice compressive strength parameter derived from the upper and lower bound estimates.

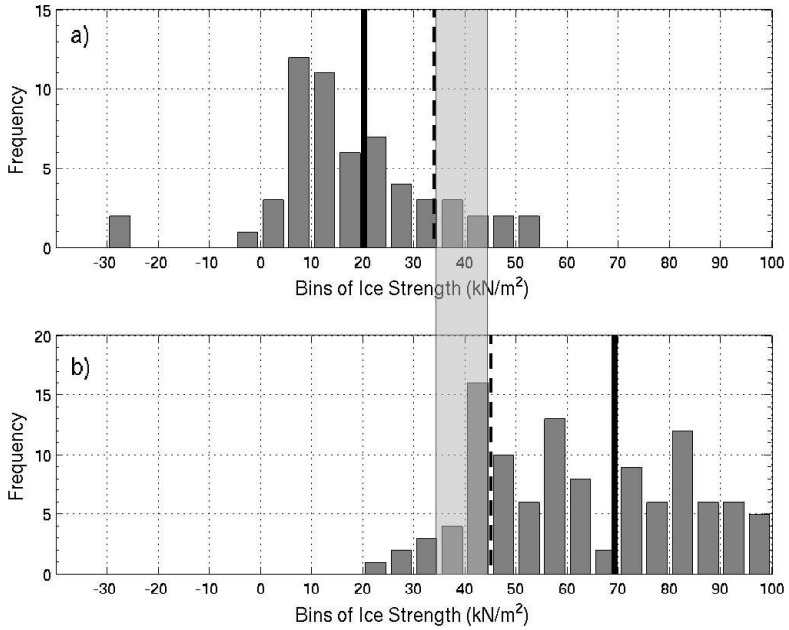

FIG. 4. Histogram of lower bound (a) and upper bound (b) estimates of sea-ice compressive strength parameter (P^*). These estimates were obtained using satellite derived sea-ice drift data from the winter (Oct-May) of 1996-97. In the top panel, tensile strength estimates are shown as negative P^*. In this case, lower bound refers to the absolute value of P^*. The thick vertical solid and dashed lines indicate the mean and, plus or minus one standard deviation for the P^* distributions. The grey shaded area indicates the range of possible sea-ice compressive strength parameters derived from the upper and lower bound estimates.